Ionics (2019) 25:1243–1257
https://doi.org/10.1007/s11581-019-02836-6

ORIGINAL PAPER

Hydration, CO_2 stability and wireless electrochemical promotion studies on yttria-doped Ba (Ce, Zr) O_3 perovskites

Efstratios Stavrakakis[1] · Matthew West[1] · Stephen Johnston[1,2] · Ronan McIlwaine[1] · Danai Poulidi[1]

Received: 24 July 2018 / Revised: 14 December 2018 / Accepted: 7 January 2019 / Published online: 24 January 2019

Abstract

$BaCe_{1-x}Y_xO_{3-\delta}$ (BCY) and $BaCe_{0.8-y}Zr_yY_{0.2}O_{3-\delta}$ (BCZY) perovskite mixed metal oxides were synthesised by an aqueous sol-gel technique to be investigated for their suitability in intermediate-temperature catalytic applications such as Electrochemical Promotion of Catalysis. The hydration capacity and the stability under CO_2 environments of the samples were studied using thermogravimetric analysis. Based on the evaluation of these properties, $BaCe_{0.6}Zr_{0.2}Y_{0.2}O_{3-\delta}$ (BCZ20Y20) was selected as the membrane support for wireless Electrochemical Promotion for CO oxidation on Pt. In a dual-chamber reactor, the use of H_2/H_2O flow in the sweep side induced promoting species supply to the catalyst in the reaction side of the reactor. Moderate promotion of the catalytic rate up to 10% was observed for temperatures up to 650 °C, while this promotional effect was reversible and repeatable. The encouraging preliminary catalytic experiments together with the membrane's stability under the applied conditions reinforce the candidacy of BCZY membranes for intermediate-temperature applications in catalytic membrane reactors.

Keywords Doped barium cerate · Sol-gel synthesis · CO_2 stability · Thermogravimetric analysis · Hydration studies · Wireless electrochemical promotion

Introduction

After Iwahara et al. [1] reported for the first time high-temperature proton-conducting ceramics, several perovskite-type oxides have been listed as potential proton conductors.

Among these, yttrium doped-barium cerate-$BaCe_{1-x}Y_xO_{3-\delta}$ (BCY) has been reported as the most prominent proton conductor [2]. Here, x amount of Y^{3+} substitutes Ce^{4+} in the $BaCeO_3$ lattice, creating a maximum of $\delta = x/2$ oxygen vacancies; the actual number of vacancies will depend on the degree of hydration and oxidation of the material under a given set of conditions. The created oxygen vacancies are therefore proportional to dopant concentration of the material and can be used for protonic transport by incorporation of hydrogen into the crystal lattice according to the following reactions (in wet and dry atmospheres respectively): proton transport involves "proton hoping" via the Grotthuss mechanism between lattice oxygen sites.

$$H_2O + V_o^{\cdot\cdot} + O_o^x \rightarrow 2OH_O^{\cdot} \quad (1)$$

$$H2 + 2O_O^x \rightarrow 2OH_O^{\cdot} \quad (2)$$

Where, according to the Kroger-Vink notation, $V_O^{\cdot\cdot}$ denotes a + 2 positively charged oxygen vacancy on the crystal lattice, O_O^x a neutral charged lattice oxygen and $OH_O^{\cdot}$ a hydroxyl group occupying an oxygen site with a + 1 charge. Depending on the conditions, Y-doping can enhance proton conductivity of $BaCeO_3$ and/or induce oxygen ion conductivity as well. At low temperatures, BCY behaves as a pure proton conductor, but at higher temperatures, there is competition between proton and oxygen ion conduction. Between 500 and 600 °C, proton conductivity dominates while for 700–800 °C this is reversed [3]. Despite its huge potential as a proton-conducting solid electrolyte, H_2-permeable membrane and H_2O-permeable membrane, BCY has been reported to be chemically unstable in CO_2 atmospheres, where the $BaCeO_3$ structure disintegrates to $BaCO_3$ and CeO_2 according to the following equation [4]:

✉ Danai Poulidi
d.poulidi@qub.ac.uk

[1] School of Chemistry and Chemical Engineering, Queen's University Belfast, Stranmillis Road, Belfast BT9 5AG, UK

[2] Present address: School of Engineering, Newcastle University, Newcastle upon Tyne NE1 7RU, UK

$$BaCeO_3 + CO_2 \rightarrow BaCO_3 + CeO_2 \quad (3)$$

Several studies [5–7] have indicated that further substitution of Ce^{4+} with Zr^{4+} results in a more chemically stable compound $BaCe_{1-x-y}Zr_yY_xO_{3-\delta}$ (BCZY) in CO_2 environments. However, it is known that zirconate-based electrolytes have a greatly reduced conductivity compared to BCY [1, 8] and the challenge lies in finding the optimum ratio between Ce^{4+} and Zr^{4+} to obtain a conductive and stable material. Other investigations [9–14] have shown that for concentrations of Zr^{4+} of 20–40% in the lattice, the chemical stability is enhanced without much expense of proton conductivity. The present study investigates the hydration properties and stability under CO_2 environments via thermogravimetric analysis of BCY and BCZY powders synthesised via an aqueous sol-gel method [15]. Several Y- and Zr-doping levels were tested in order to produce a material that can be applicable and simultaneously effective for electrocatalytic applications, in particular Electrochemical Promotion of Catalysis (EPOC) reactions of environmental importance. In EPOC, a conducting support can be used in spontaneous reactions to activate and tune a heterogeneous catalyst to an extent that is higher than the value predicted by Faraday's law. Specifically, the activity and the selectivity of metal catalysts interfaced with an ionically conducting support can be modified in situ and reversibly by the application of small currents or potentials between the catalyst film and an auxiliary electrode. The phenomenon has been recently summarised in a number of reviews [16, 17]. In addition, for supports with mixed ionic and electronic conductivity (such as BCZY), a wireless configuration has also been proposed by Poulidi et al. [18–23] utilising a chemical potential difference of the promoting species across a dense membrane supporting the catalyst. Wireless EPOC has been observed using both mixed oxygen ion and electronic conductors [18–22] or mixed protonic and electronic conductors [23] in different reactor configurations. In this work, the most promising composition of BCZY evaluated in terms of stability under CO_2 environments was used for the wireless EPOC of CO oxidation on a Pt catalyst. This is the first attempt to electrochemically promote a catalytic reaction with the use of a BCZY membrane and without an external circuit. Due to low electronic conductivity within the tested temperature range (350–750 °C), these membranes present limited hydrogen permeation fluxes, i.e., in the order of magnitude of 10^{-3}–10^{-2} mL cm^{-2} min^{-1} in the thickness range of 1–1.5 mm [24] that is commonly used in EPOC studies. However, EPOC activation can be achieved even with very small current densities of the order of microampere per square meter (μA cm^{-2}) [25], equivalent to protons flux of the order of 10^{-4} mL cm^{-2} min^{-1}.

Experimental

Powder synthesis

$BaCe_{1-x}Y_xO_{3-\delta}$ (BCY) and $BaCe_{0.8-y}Zr_yY_{0.2}O_{3-\delta}$ (BCZY) compounds where $x = 0.05$, 0.1 and 0.2 (BCY5, BCY10 and BCY20, respectively) and $y = 0.1$, 0.2 and 0.4 (BCZ10Y20, BCZ20Y20 and BCZ40Y20, respectively) were synthesised via aqueous sol-gel technique according to the method proposed by Chen et al. [15]. The raw materials $BaCO_3$ (≥ 99%, Sigma-Aldrich), CeO_2 (≥ 99.9%, Aldrich), Y_2O_3 (≥ 99.99%, Aldrich) and ZrO_2 (≥ 99%, Aldrich) were dissolved in 500 ml deionised H_2O. The final solution was formed by adding 153 ml H_2O_2 (30% wt in H_2O, Sigma-Aldrich) and 5.3 ml of ammonia (25%, Sigma-Aldrich). After stirring for 2 h and drying at 90 °C until complete evaporation, the xerogel was heated at 250 °C for 2 h. BCY samples (without Zr content) were calcinated at 1100 °C for 5 h and BCZY samples at 1250 °C for 10 h or 1400 °C for 24 h. X-ray diffraction (XRD) analysis (not shown here) showed that temperatures lower than 1100 °C showed traces of the BaCe3 phase and therefore were not explored further. For the BCZY samples, a range of calcination temperatures was employed, and in this work, we show results obtained from the lowest (1250 °C) and typical (1400 °C) calcination temperatures required to achieve pure phase. Finally, the powder was ground and sieved for particle size < 63 μm.

Powder characterisation

The powders were characterised through XRD analysis; the corresponding patterns were collected in a Panalytical X'Pert PRO Diffractometer at room temperature. Identification of the crystalline phases was obtained via Panalytical X'pert Highscore Plus software, equipped with the ICSD database.

Hydration experiments were performed by thermogravimetric analysis (TGA) using a TGA Q5000 V3.17 Build 265 Instrument. The first step for all tested samples included an initial drying/dehydration step which consisted of heating the sample from room temperature to 1000 °C at a ramp rate of 10 °C min^{-1} under a flow of 25 ml min^{-1} N_2 and then cooling down (using the same ramp rate and flow conditions) to the starting temperature of the hydration experiments. Following this step, dynamic TGA experiments were run from 100 to 700 °C at a ramp rate of 10 °C min^{-1}, while isothermal experiments were run at 450 °C for a period of 6 h. These experiments were carried out for all BCY and BCZY powders. During the 'hydration steps', the nitrogen stream was humidified through a glass bubbler filled with water. The glass bubbler was kept to the laboratory temperature which was ca. 20 °C with a corresponding vapour pressure of 2.3 kPa.

Chemical stability was tested through three different methods of TGA. The BCY samples were tested only through

the first method, while for the BCZY samples, all three methods were used. In all cases, the samples were heated from 30 to 1000 °C and subsequently were cooled from 1000 °C to the initial temperature of each method with a 10 °C min^{-1} temperature ramp rate and under 25 ml min^{-1} N_2 flow. The first two methods consisted of heating the sample from 100 to 1000 and 100–600 °C at 10 °C min^{-1} and 5 °C min^{-1}, respectively. The third method included isothermal exposure in CO_2 for 5 h at 400, 450, and 500 °C. In all cases, a flow rate of 25 ml min^{-1} of pure CO_2 was used. Finally, the degree of materials decomposition was evaluated again via XRD at room temperature.

Fabrication of Pt/BCZY/Pt catalytic membrane

The assessment of hydration and CO_2 stability for the in-house synthesised powders aimed for selecting a suitable composition for further catalytic work. Once this was identified as $BaCe_{0.6}$ $Zr_{0.2}Y_{0.2}O_{3-\delta}$ (as will be discussed in the following section), the powder was supplied by a commercial provider (Marion technologies). This was done so that there would be no differences in batch characteristics between different samples used for the fabrication of membrane pellets. For the preparation of these membranes, a mixture consisting of 1.2 g of BCZ20Y20 powder and 2 wt% of ZnO nanopowder (544906 Aldrich), used as the sintering aid, was uniaxially pressed in a pellet die (19.5 mm internal diameter) under 5 t for 2 min. The disk membranes (15 mm in diameter, 1.2 mm in thickness) were obtained by sintering in a Microwave Furnace (Analytix Pyro Muffle Furnace) at 1150 °C and 1800 W for 6 h. The sintered samples (Fig. 1) had a relative density of ca. 92%, as measured by Archimedes method and compared to the theoretical density of BCZ20Y20 provided by the supplier, i.e. 6.18 g cm^{-3}.

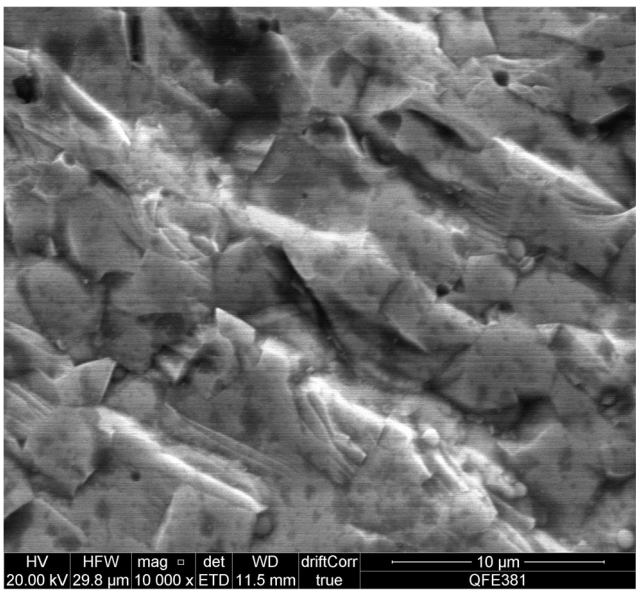

Fig. 1 SEM image of the fracture section of BCZ20Y20 membrane prepared by microwave sintering at 1150 °C

Circular platinum films with 7 mm diameter were fabricated in both sides of the BCZY disk after brush-painting with a Pt paste and firing at 800 °C for 30 min. This paste was prepared by dissolving $H_2PtCl_6 \cdot 6H_2O$ powder (206083, Sigma-Aldrich) in isopropanol and terpinol-based ink vehicle (Fuel Cell Materials). The Pt load for each film was approximately 5 mg, while the geometric projected surface area was 0.42 cm^{-2}.

Catalytic experiments

Catalytic experiments on CO oxidation using a wireless Electrochemical Promotion configuration were conducted in a dual-chamber membrane reactor comprising of a BCZY dense pellet membrane separating the two reactor chambers. The reaction took place in one chamber of the reactor while the other chamber was used for the sweep gas that controlled the migration of promoting species to and from the catalyst surface area. The wireless EPOC reactor and experimental method have been described in detail in work by Poulidi et al. [18] and a similar setup was used in this work. The probe reaction was carried out at different temperatures, i.e. 350, 550, 650 and 750 °C using a total flow rate of 200 ml min^{-1}. The partial pressures of CO and O_2 in the reaction chamber were at 1 and 10 kPa, respectively. The balance of the reaction mixture was He. The purpose for using excess of oxygen is to prevent carbon deposition and subsequent poisoning of the catalyst. The unmodified reaction rate was obtained using Ar in the sweep side of the reactor, while protonic species were supplied to the catalyst in order to promote the catalytic activity via the use of a 15% H_2/2.3% H_2O (balance Ar, total flow rate 100 ml min^{-1}) sweep on the reaction side. The use of different balance gases in the reaction and sweep sides allowed for the detection of leaks (not observed for the duration of these experiments). A Vaisala GMP343 CO_2 analyser was connected to the reacting chamber outlet to measure the concentration of produced CO_2. The reaction rate was calculated in micromole per second per square centimetre, i.e. CO_2 production rate over the projected catalytic surface area.

Stability of BCZ20Y20 membrane

The stability of the membrane in the applied conditions during the catalytic tests was evaluated through XRD. Due to experimental difficulties for detaching/re-attaching the used membrane from/on the reactor, a similar Pt/ BCZ20Y20/Pt membrane was placed in a single-chamber reactor and exposed in similar conditions for 24 h at each tested temperature.

Results

Synthesis

The XRD patterns of all the prepared samples are presented in Fig. 2a. A pure perovskite phase was obtained in every case and there were no appearance of peaks related to the precursors or secondary phases. However, the shoulders on the main peaks of BCZ40Y20 indicated the existence of a very minor perovskite phase with slightly smaller lattice. Similar 'shoulders' were observed by Della Negra et al. [26] for similar Zr-doping, i.e. $BaCe_{0.5}Zr_{0.4}Y_{0.1}O_{2.95}$ calcined at 1400 °C, as well as by Fabbri et al. [27] for $BaCe_{0.5}Zr_{0.3}Y_{0.2}O_{2.9}$ and $BaCe_{0.3}Zr_{0.5}Y_{0.2}O_{2.9}$. Figure 2b shows a closer view of the peak between 50° and 53° in order to highlight the effect of Y- and Zr-doping on the XRD pattern and the induced peak shift. For BCY samples and higher substitution of Y^{3+}, the main peaks are retained at the same angle. This comes in disagreement with the fact that the higher ionic radius of the dopant Y^{3+} ions ($R^{III} = 0.9$ Å) in comparison to this of the substituted Ce^{4+} ($R^{IV} = 0.87$ Å) [28] should have resulted in increased d-spacing and consequently (due to Bragg's law) in decreased angles of the peak positions. However, Knight et al. [29] previously reported that for low level of Y-doping, the crystal system and the space group of barium cerate are retained with a very limited effect, because of the good match between the effective ionic radius of Y^{3+} and Ce^{4+}. A shift in higher angles was observed in the peak positions of BCZY samples increasing the Zr content against Ce. This can be justified by the smaller ionic radius of the six-coordinated Zr^{4+} ions ($R^{IV} = 0.72$ Å) when compared to that of Ce^{4+} [28]. The effect of the calcination treatment on the structure of BCZY powder is shown in Fig. 3. Calcination at 1250 °C for 10 h did not result in a single perovskite phase. A $BaZrO_3$ phase existed in all BCZY samples, while for higher amount of Zr dopant, a ZrO_2 phase was also formed possibly due to excess of Zr^{4+}. Calcination at 1400 °C for 24 h led to the formation of the required Ba-Ce-Zr-Y oxide phase with no significant presence of secondary phases.

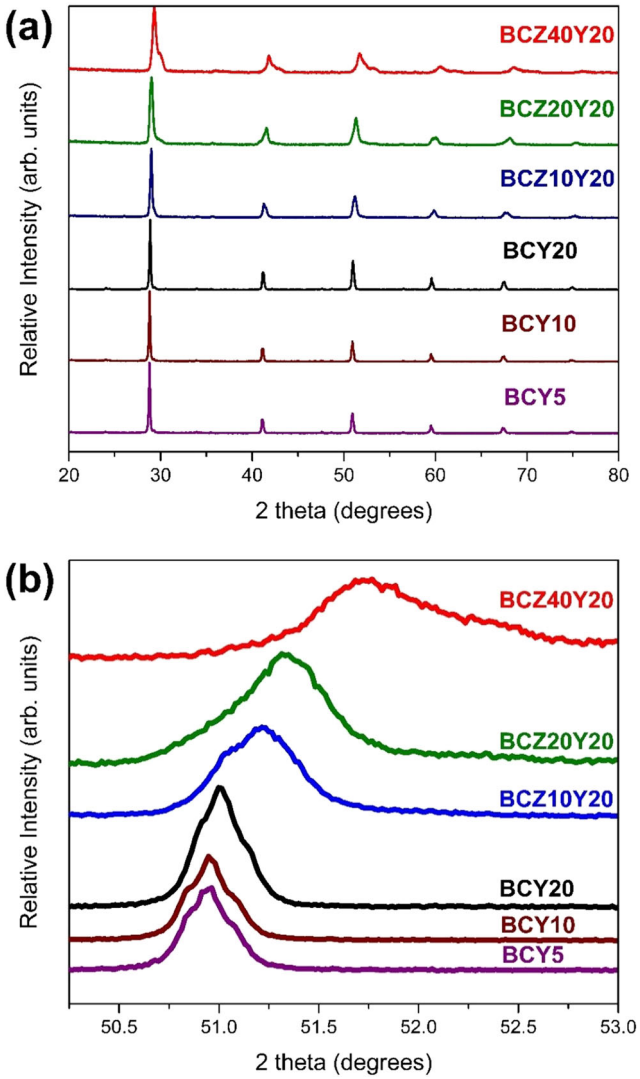

Fig. 2 **a** XRD patterns for BCY samples prepared at 1100 °C (5 h) and BCZY samples prepared at 1400 °C (24 h) and **b** enlarged view of peaks between 50° and 53°

Water uptake experiments

The hygroscopic behaviour of the BCY powder was studied first using a heating rate 10 °C min^{-1} from ~ 30 to 700 °C as described earlier and is shown in Fig. 4. The initial treatment with 'dry' N_2 (not shown here) was sufficient to fully dry the powder. In theoretical basis, the maximum water uptake should be linearly depended on the Y-substitution and the oxygen vacancy concentration (1/2 oxygen vacancy per dopant ion) [30]. In our experiments, the direct relation between Y-doping concentration and hydration capacity was confirmed. Higher Y-content on the B-site resulted in an increase in the water uptake and BCY20 exhibited the highest weight gain of 0.4%. By assuming a one-to-one relation (on a molar basis) between water uptake and oxygen vacancies, the theoretical maximum water uptake which corresponds to 100% of the oxygen vacancies for BCY5, BCY10 and BCY20 is 0.14, 0.28 and 0.57 wt%, respectively. Hence, the protonic defect concentration was measured as 60, 54 and 70% of full capacity for BCY5, BCY10 and BCY20, respectively. However, these values were lower than others reported in the literature [31–33] possibly due to relatively high heating rate used in this work. It has been shown that the dehydration temperature decreases with lower Y-content [31, 34], and thus, the heating rate of 10 °C min^{-1} did not allow the samples with the lower Y-content to reach their full hydration potential. For this reason, we decided to also investigate the isothermal water uptake at 450 °C (shown in Fig. 5), which is a temperature of interest for EPOC applications in particular that are of interest to our group. In this case, the protonic defect concentration

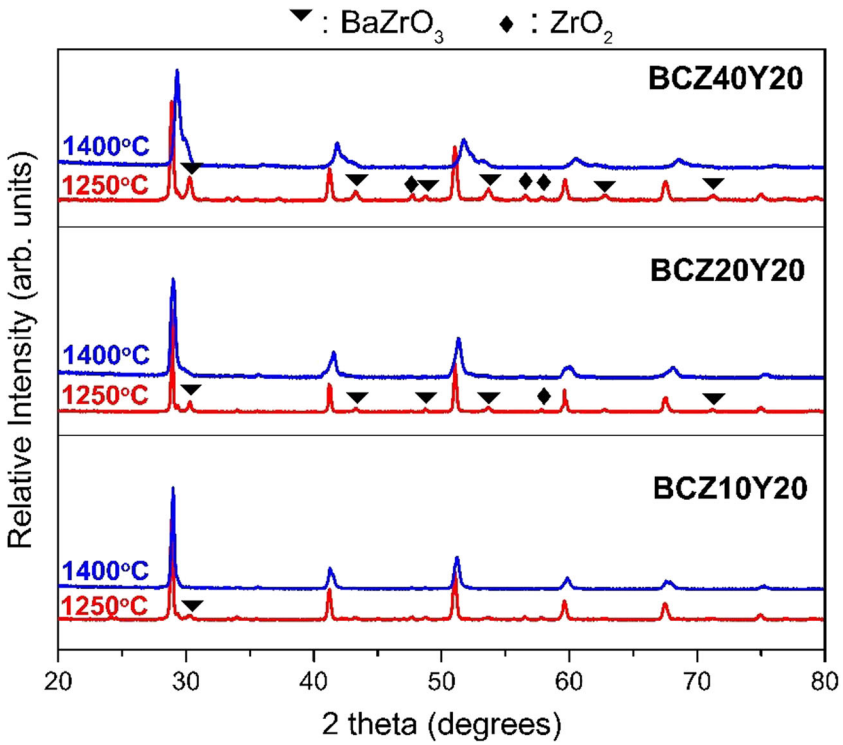

Fig. 3 XRD patterns for BCZY samples calcined at 1250 °C for 10 h (red line) and 1400 °C for 24 h (blue line)

was almost independent on the Y-content and values of more than 80% saturation were obtained for all BCY samples (illustrated by the red line in Fig. 5a). These results were in a good agreement with data presented by Kruth et al. [24] (ca.80% $\left[OH_O^{\cdot}\right]$ for BCY5 and BCY10). Ricote et al. [25] and Oichi et al. [26] presented slightly higher values during isothermal measurements, but this could be related to different flow conditions (oxidising atmospheres) used in their work. Taking into account these results, it was decided to test Zr^{4+} substitution on Ce^{4+} only for BCY20 which presented the highest hydration capacity and fastest respond to hydration that is associated with high protonic conductivity. The effect of Zr-doping on the BCY20 water uptake capability at 450 °C is shown in Fig. 5b. The amount of water that was incorporate in the lattice gradually decreased with Zr content and $\left[OH_O^{\cdot}\right]$ took values 81, 79, 54 and 28% for $y = 0$, 0.1, 0.2 and 0.4,

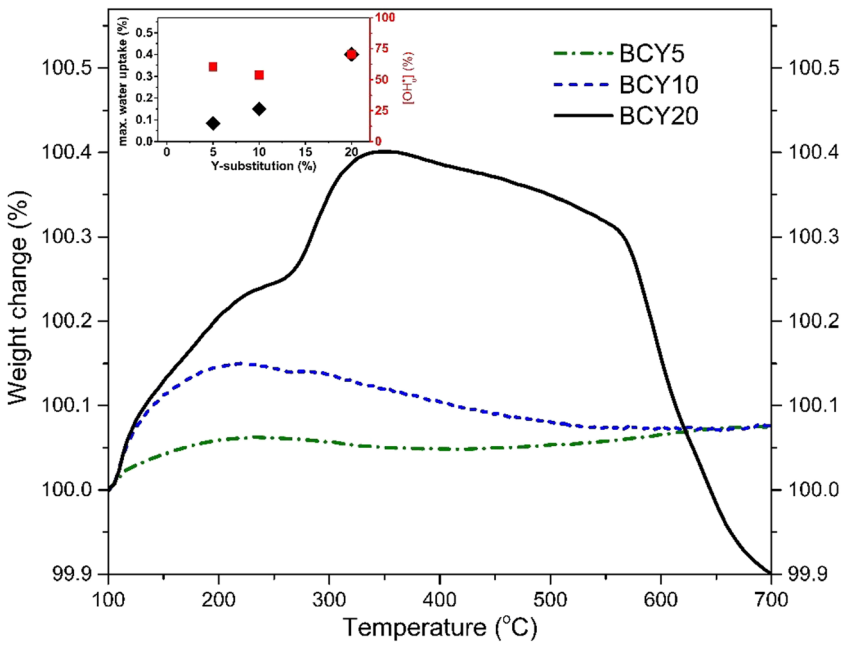

Fig. 4 Hydration TGA of varying Y-dopant level BCY on heating up to 700 °C in 3%H_2O/N_2. The maximum water uptake (black) and percentage of filled oxygen vacancies (red) in respect to the Y-content are presented in the embedded chart

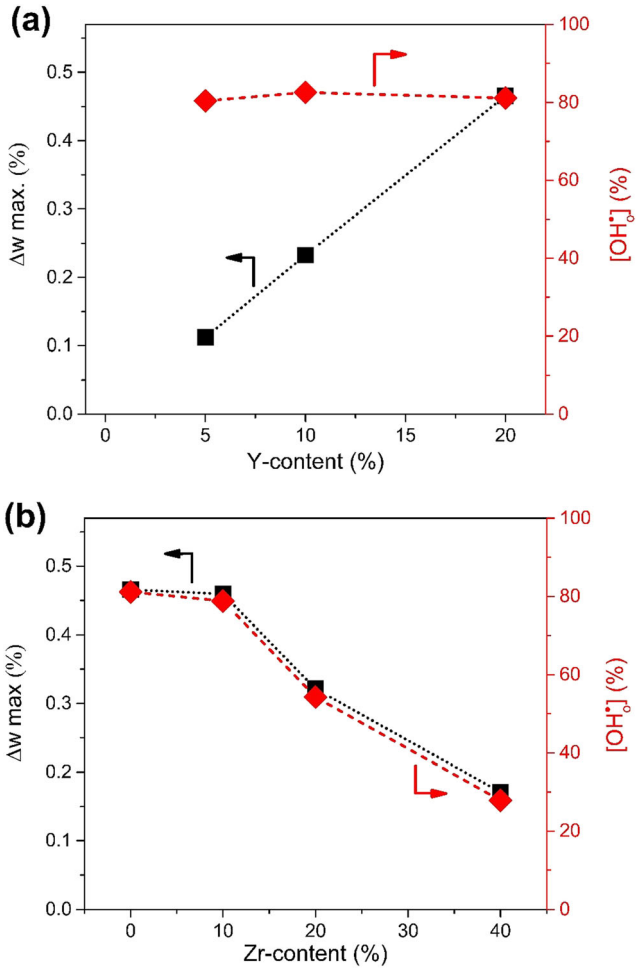

Fig. 5 Water uptake (black line) and percentage of filled oxygen vacancies (red line) of **a** $BaCe_{1-x}Y_xO_{3-\delta}$ ($x = 0.05$, 0.1 and 0.2) and **b** $BaCe_{0.8-y}Zr_yY_{0.2}O_{3-\delta}$ ($y = 0$, 0.1, 0.2 and 0.4) powders during isothermal TGA at 450 °C in $3\%H_2O/N_2$

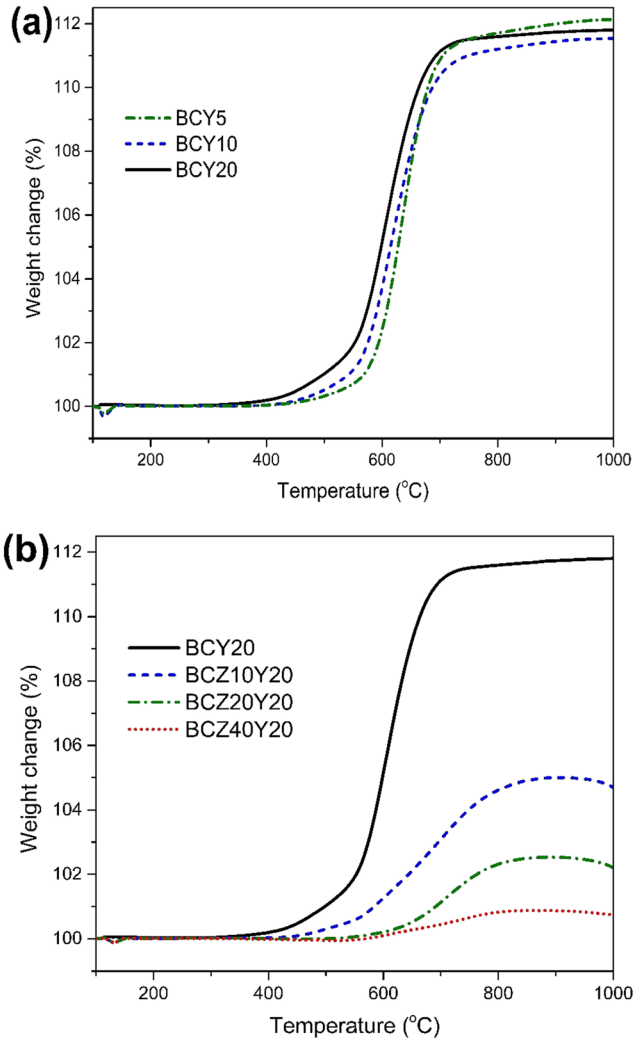

Fig. 6 TGA using a heating rate of 10 °C min^{-1} up to 1000 °C in CO_2 for **a** $BaCe_{1-x}Y_xO_{3-\delta}$ ($x = 0.05$, 0.1 and 0.2) and **b** $BaCe_{0.8-y}Zr_yY_{0.2}O_{3-\delta}$ ($y = 0$, 0.1, 0.2 and 0.4) powders

respectively. Higher content of zirconium decreases the difference in electronegativity of the cations in the B-site of the perovskite lattice and consequently the hydration enthalpy becomes more negative [35]. Thus, the proton concentration should decrease with higher zirconium content when hydration is tested at a specific temperature. Same behaviour was reported by Ricote et al. [25] but with a lower expense in protonic defect concentration for increasing Zr-doping.

Chemical stability in CO_2 atmospheres

The chemical stability of the BCY and BCZY powders was tested in a CO_2 environment (100%) for temperatures up to 1000 °C, as shown in Fig. 6. All the samples were stable up to approximately 400 °C. Increasing level of Y-doping induced a decrease in the decomposition onset temperature and a slight improvement in stability up to ca. 700 °C, while the final weight gain was similar for all compositions, i.e. 11.5–12% (Fig. 6a). For the BCZY powders, the decomposition onset temperature increased with Zr content (from 400 to 700 °C), while the overall CO_2 weight gain showed a decreasing trend. BCZ40Y20, in particular, was extremely stable under these conditions, while for BCZ20Y20, a weight gain of only ca. 2% was obtained after 600 °C.

Virkar et al. [36, 37] have correlated the stability of perovskites with the Goldschmidt tolerance factor, t, which is parameter that describes the distortion of the structure from the ideal cubic perovskite structure and defined as:

$$t = \frac{r_A + r_O}{\sqrt{2}(\bar{r_B} + r_O)} \quad (4)$$

where r_A, $\bar{r_B}$ and r_O are the ionic radius of A, B and O atoms in the lattice. Perovskites with values of tolerance factor that approaching unity are more stable. According to the calculated tolerance factor values for all the tested materials (Table 1), the stability test presented in Fig. 5 confirms this theory.

Table 1 Tolerance factor for materials used in this work

Sample	Tolerance factor, t
$BaCe_{0.95}Y_{0.05}O_{2.975}$	0.85606
$BaCe_{0.9}Y_{0.1}O_{2.95}$	0.85550
$BaCe_{0.8}Y_{0.2}O_{2.9}$	0.85437
$BaCe_{0.7}Zr_{0.1}Y_{0.2}O_{2.9}$	0.86004
$BaCe_{0.6}Zr_{0.2}Y_{0.2}O_{2.9}$	0.86578
$BaCe_{0.4}Zr_{0.4}Y_{0.2}O_{2.9}$	0.87750

The same behaviour to that discussed previously (Fig. 6b) for the BCZY samples was observed for a slower heating rate (5 °C min^{-1}) and a narrower temperature range (up to 600 °C); this data is not shown here. Next, the powders were tested in CO_2 atmospheres through isothermal TGA at three different temperatures: 400, 450 and 500 °C for 5 h which is approximately equal to the duration of a typical EPOC experiment. The weight gain at the end of each run is shown in Fig. 7. The hypothesis of zirconium effect on stability was confirmed for this case as well, but the remarkable feature was that BCZ20Y20 presented high stability and equivalent to this of BCZ40Y20 at 400 and 450 °C. The summary of these experiments including quantification of decomposition in [$BaCO_3$] % is given in Table 2. These results are in a very good agreement with other similar studies; for example, Sawant et al. [11] recorded ca. 1.25% and ca. 2.25% weight gain for BCZ40Y20 and BCZ40Y20, respectively, after a dynamic TGA from 100 to 900 °C with a 10 °C min^{-1} heating rate. In the present study, the values for the same samples in the experiment with same conditions corresponded to ca. 0.5% and ca. 2 wt%, respectively.

The conclusions drawn from the above experiments were strengthened by XRD analysis presented in Fig. 8, where the XRD patterns of the fresh samples were compared with those of the samples after all the TGA experiment under a flow of CO_2. For the sample without Zr-doping, BCY20, there was decomposition even after 600 °C, while after 1000 °C or 5 h at 500 °C, extended presence of $BaCO_3$ and CeO_2 phases were identified in the structure and the main peaks of perovskite structure disappeared. Zirconium substitution of 10% in the B-site resulted in significant appearance of these phases only after heating up to 1000 °C to CO_2. No actual changes in the structure of BCZ20Y20 and BCZ40Y20 were observed in both cases, confirming the great stability of these materials in CO_2 exposure.

The thermogravimetric data obtained for the reaction of BCZY with CO_2 were analysed further to evaluate the decomposition reaction kinetics. Activation energy values, E_a, were determined by two different methods for the Zr-substituted samples. Evaluation of reaction kinetics for each composition was accomplished by Kissinger's method [38], where the change of the temperature (corresponding to the maximum reaction rate) is described as a function of different heating rates, according to the following equation:

$$\ln\left(\frac{\beta}{T^2}\right) = \ln\frac{AR}{Ea} - \frac{Ea}{RT} \tag{5}$$

where β is the value of the constant heating rate, A is the Arrhenius pre-exponential factor, T is the temperature that

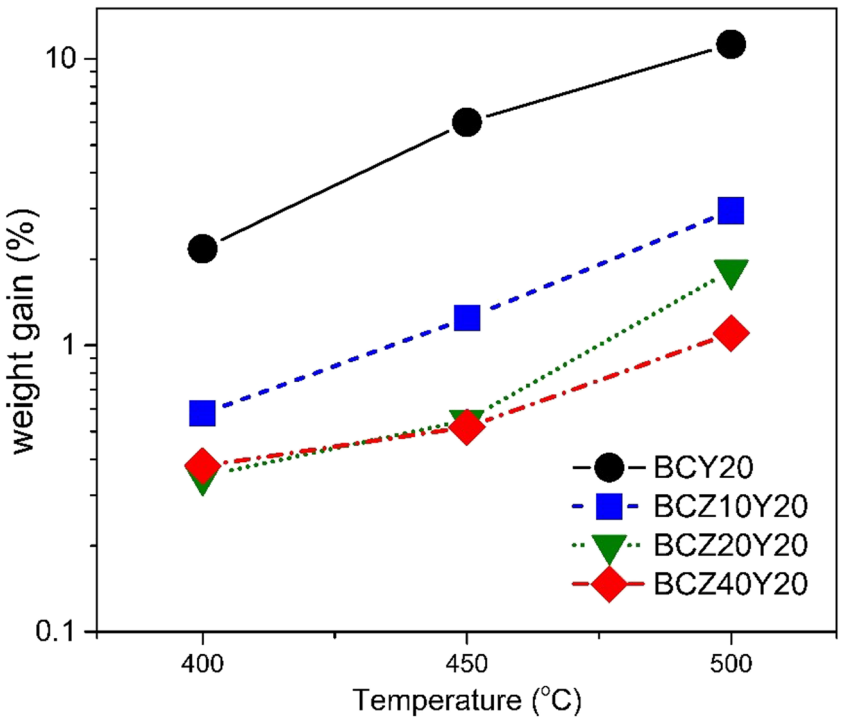

Fig. 7 Weight gain of $BaCe_{0.8-y}Zr_yY_{0.2}O_{3-\delta}$ ($y = 0$, 0.1, 0.2 and 0.4) powder during isothermal TGA at 400, 450 and 500 °C in CO_2

Table 2 Weight gain and % mol $BaCO_3$ formation for BCZY powder during TGA experiments in CO_2

	$BaCe_{0.8}Y_{0.2}O_{2.9}$		$BaCe_{0.7}Zr_{0.1}Y_{0.2}O_{2.9}$		$BaCe_{0.6}Zr_{0.2}Y_{0.2}O_{2.9}$		$BaCe_{0.4}Zr_{0.4}Y_{0.2}O_{2.9}$	
Conditions	Δw %	[$BaCO_3$] %	Δw %	[$BaCO_3$] %	Δw %	[$BaCO_3$] %	Δw %	[$BaCO_3$] %
100 °C → 600 °C[a]	7.38	52.59	2.06	14.47	0.46	3.19	0.34	2.25
100 °C → 1000 °C[b]	11.81	84.14	5.00	35.08	2.54	17.53	0.88	5.86
5 h at 400 °C	2.17	15.50	0.58	4.06	0.35	2.41	0.38	2.53
5 h at 450 °C	6.01	42.86	1.24	8.72	0.55	3.79	0.52	3.46
5 h at 500 °C	11.24	80.14	2.95	20.70	1.83	12.63	1.10	7.35

[a] 5 °C/min

[b] 10 °C/min

corresponds to the maximum reaction rate and R is the gas constant. Assumption for first-order reaction was made so that Eq. (5) is valid. A previous study [39] has shown that application of Kissinger's formula even in other than first-order kinetic models leads to only a less than 5% deviation from the actual activation energies for values of (E_a/RT) greater than 10. Hence, the TGA data collected for the scans of 5 °C min^{-1} to 600 °C and 10 °C min^{-1} 1000 °C in CO_2, as

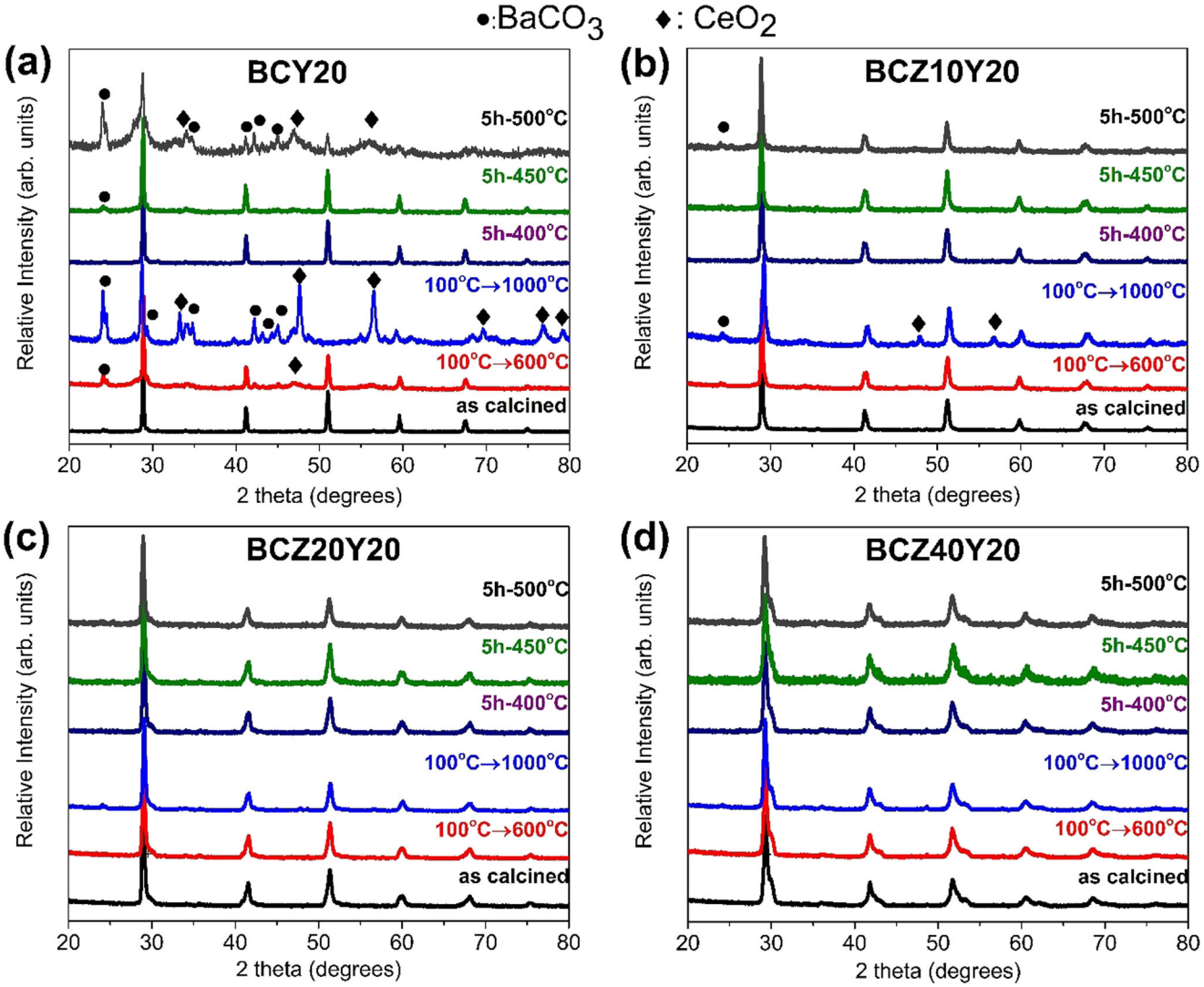

Fig. 8 XRD patterns of BCZY powder obtained at room temperature after calcination (black line), after 5 °C/min heating up to 600 °C in CO_2 (red line), after 10 °C/min heating up to 1000 °C in CO_2 (blue line) and after 6 h at 400 °C (purple line), 450 °C (green line) and 500 °C (grey line)

presented in Fig. 7, was used with Eq. 5. Figure 9a shows the plots of $\ln(\beta/T^2)$ versus $1/T$ for each composition and the slope of this lines corresponds to $-(E_a/R)$ values. Zirconium addition gradually decreased the reaction activation energy from 177 to 53 kJ mol^{-1} and increased perovskite resistance against CO_2.

For the second method of activation energy determination, the isothermal TGA data was applied to the Jander model [40]. This model has been widely used to analyse kinetics of gas-solid reactions controlled by cation diffusion (such as Ba^{2+} in the present case). Also, it has been already applied to define the effect of Zr-doping on the apparent rate constant, k, and the activation energy of the BCZY decomposition reaction [41]. Using this model, the weight changes, Δw, of BCY20 and the different BCZY samples obtained during the isothermal TGA experiments at 400, 450 and 500 °C in CO_2 were converted to reaction rate ratio, α, according to the following equation:

$$a = \frac{\Delta w}{w_{\text{tot}}} \tag{6}$$

where w_{tot} is the theoretical maximum weight gain if BCZY was completely decomposed. The reaction kinetics are described by Jander's function as follows:

$$f(a) = \left[1-(1-\alpha)^{\frac{1}{3}}\right]^2 = k't \tag{7}$$

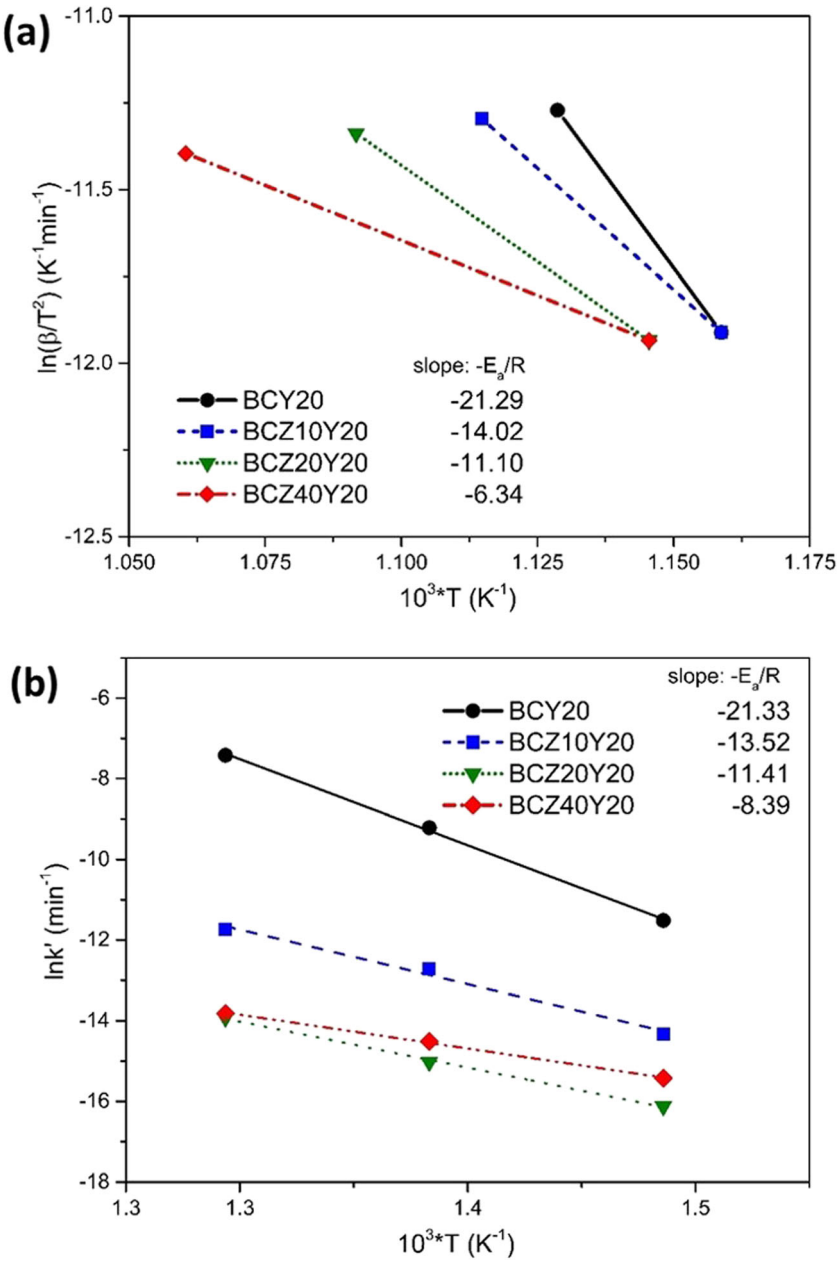

Fig. 9 Arrhenius plot for $BaCe_{0.8-y}Zr_yY_{0.2}O_{3-\delta}$ ($y = 0, 0.1, 0.2$ and 0.4) decomposition in 1 atm of CO_2. **a** Using Kissinger's model and **b** using the Jander model

After weight changes were converted to reaction ratios, $\left[1-(1-\alpha)^{\frac{1}{3}}\right]^2$ was plotted against time to estimate k' as the slope of each line (Fig. 9b). The results of the kinetic analysis by the two methods are presented in Table 3. Similar values of activation energies were determined using both methods for all the sample with the exception of BCZ40Y20 where a more significant variation between the two methods was observed. The deviation between the two calculations of the activation energies for this material is probably rationalised by the aforementioned limitation of Kissinger's method since for this sample the value of (E_a/RT) was not higher than 10. According to this data, Zr-doping reduces the energy barrier for BCZY decomposition; however, the reactivity with CO_2 is restricted as the pre-exponential factor, A, is diminished by several orders of magnitude for increasing Zr content. Similar findings were reported by Okiba et al. [41] who employed Jander method and analysed the kinetics of Zr-doped $BaCe_{0.9}Y_{0.1}O_{3-\delta}$ with CO_2: activation energies were reduced from 213 to 79 kJ mol^{-1} with Zr substitution between 0 and 30%.

Overall, while both BCZ20Y20 and BCZ40Y20 both showed excellent stability under CO_2 environments, it was decided to move forward with the composition containing less Zr (i.e., BCZ20Y20) due to the better hydration and sinterability of this material.

Wireless electrochemical promotion of CO oxidation on a Pt/BCZY catalyst

BCZ20Y20 was used for proof-of-concept experiments on wireless EPOC using CO oxidation on a Pt catalyst as the probe reaction. The catalytic experiments were performed at 350, 550, 650 and 750 °C and the corresponding dynamic reaction rate transients for a series of alternant Ar-H_2/H_2O sweeps are shown in Fig. 10. At the beginning of each experiment, the catalyst was left under reaction conditions for a period of 12 h in order to obtain a stable rate (using an Ar-sweep on the sweep side).

Upon introduction of the H_2/H_2O flow on the sweep side of the reactor, a chemical potential difference of hydrogen species across the membrane is created. This will act as the driving force for these species to migrate across the membrane and spillover on the catalyst surface to impose a similar modification to the catalytic rate as in classic EPOC [18–20]. The effect on the catalytic rate (promotion or poisoning) depends on the nature of the promoting species (electronegative and electropositive) and the adsorption status of the reactants. In the present case where a high oxygen excess is used, the oxygen coverage on the catalyst is expected to be predominant. Therefore, the catalytic rate could be promoted by enhancing the adsorption of CO through the presence of an electronegative promoter; CO acts as the electron donor in the presence of the strongly electronegative oxygen [42]. The prevailing mechanism in oxidation reactions with a proton conductor suggests that EPOC effect is due to the formation of hydroxyl-promoting species on the catalytic surface. According to this theory, protons migrate via the Grotthuss mechanism from the solid electrolyte to the catalyst/gas interface, where they form a promoting hydroxyl group through reaction with absorbed O atoms [43].

Figure 10a shows the catalytic rate transients at 350 °C where the reaction rate stabilised at an approximate value of 0.87 μmol s^{-1} cm^{-2} under Ar-sweep. Upon introduction of the H_2/H_2O flow on the sweep side of the reactor, an increase in the reaction rate was observed. This was in the form of a sharp increase (possibly an artefact due to the back pressure created by the switch to the new sweep gas) followed by a gradual settling to a new (higher than the Ar-sweep rate) steady-state value of approximately 0.9 μmol s^{-1} cm^{-2}, constituting a modest 3.4% rate increase. This promoted rate was sustained for the duration of the H_2/H_2O-sweep (in excess of 10 h). The promotion on the catalytic rate promotion can be correlated to the features previously discussed: proton migration to the catalytic surface would form hydroxyl species (electronegative promoters) which increase adsorption of the electron donor (CO). Due to the high excess of oxygen in the reactor, the reaction would be positive order to CO and thus the rate is increasing. Upon return to an Ar-sweep, the reaction rate almost returned to the original value of the unpromoted state, ca. of 0.87 μmol s^{-1} cm^{-2}. It is interesting to note that the phenomenon is rapidly reversed upon re-introduction of the Ar-sweep. This is very different from the behaviour previously

Table 3 Activation energies E_a and pre-exponential factors for BCZY reaction with CO_2 determined by the two models

Sample	E_a[a] for decomposition in CO_2 (KJ mol^{-1})	A[a] for decomposition in CO_2 (min^{-1})	E_a[b] for decomposition in CO_2 (KJ mol^{-1})	A[b] for decomposition in CO_2 (min^{-1})
$BaCe_{0.8}Y_{0.2}O_{2.9}$	177	7.43E+06	177	6.00E+08
$BaCe_{0.7}Zr_{0.1}Y_{0.2}O_{2.9}$	117	1.07E+03	112	3.46E+02
$BaCe_{0.6}Zr_{0.2}Y_{0.2}O_{2.9}$	92	2.43E+01	95	2.26E+00
$BaCe_{0.4}Zr_{0.4}Y_{0.2}O_{2.9}$	53	5.91E-02	70	5.25E-02

[a] Kissinger model

[b] Jander model

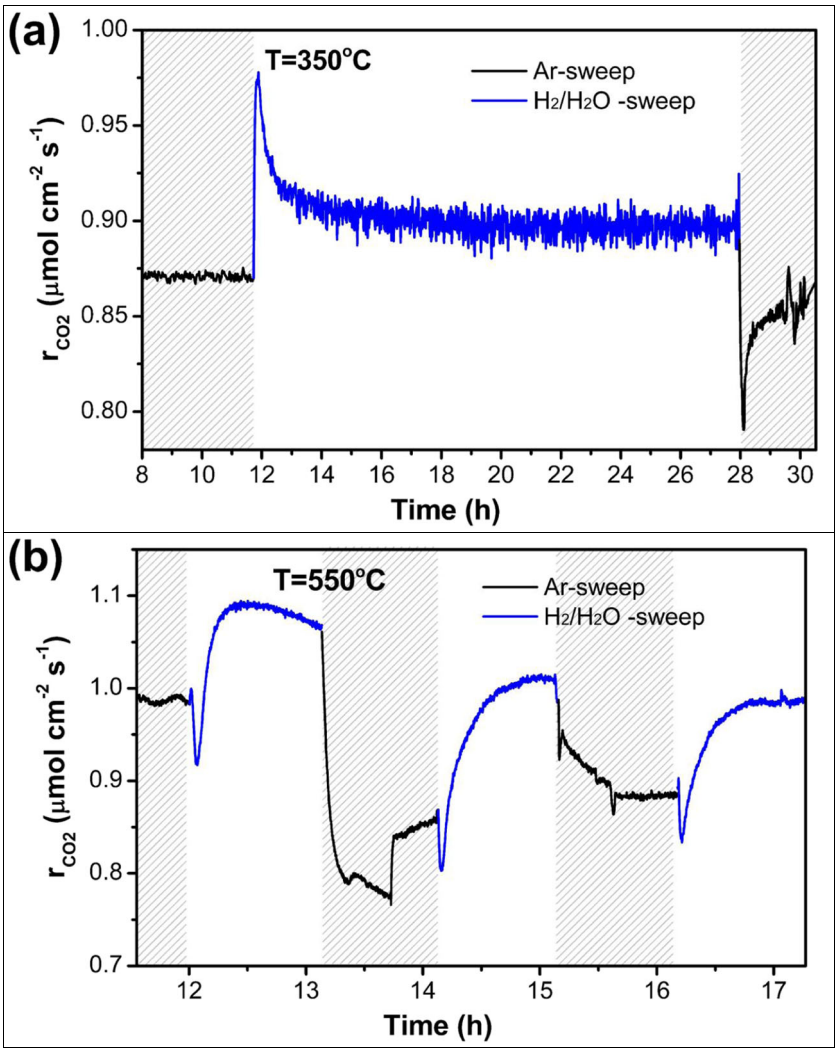

Fig. 10 Wireless EPOC of CO oxidation using a BCZY membrane in a dual-chamber membrane reactor configuration at **a** 350 °C, **b** 550 °C, **c** 650 °C and **d** 750 °C . Reactor conditions: pCO = 1 kPa, pO_2 = 10 kPa, f_{react} = 200 ml min^{-1}, f_{sweep} = 100 ml min^{-1}

observed in wireless EPOC experiments for mixed oxygen and electronic conductors [18–22] but similar to that observed for the case of a mixed protonic electronic conductor ($Sr_{0.97}Ce_{0.9}Yb_{0.1}O_{3-\alpha}$) [23] used for the modification of Pt catalytic activity for ethylene oxidation. In the case of the mixed oxygen-electronic conductor, the catalytic rate remained to the promoted state upon re-introduction of the inert gas sweep, while in the case of the mixed proton-oxygen ion conductor, there was also a rapid restoration. This fact suggest that the promoting species are possibly the same in both cases of protonic conductors, while it points away for the possibility of any oxygen ion mobility for the BCZY support at this temperature.

The reaction follows similar behaviour at 550 and 650 °C as shown in Fig. 10b, c. The imposition of the H_2/H_2O-sweep results in a ca. 5 and 10% rate increase at 550 and 650 °C, respectively. In these experiments, three cycles of Ar-H_2/H_2O sweep steps were performed in order to investigate the repeatability of the phenomenon. The use of the H_2/H_2O-sweep results in a ca. 5 and 10% rate increase at 550 and 650 °C, respectively, and upon the use of Ar-sweep, the reaction rate tended to drop close to the original unpromoted value. The observed rate increase was of a similar magnitude for all three cycles of each experiment at these temperatures although there was a gradual decline of the overall catalytic rate after each cycle.

A very different behaviour was observed for the catalytic experiment at 750 °C (Fig. 10d). During the first H_2/H_2O-sweep, the reaction rate decreased and then upon the re-introduction of Ar-sweep decreased further to stabilise at a lower value. Further cycles did not have any effect on the reaction rate. It is known that the conductive properties of BCZY are gradually changed with the elevation of temperature and the oxygen ion conductivity becomes dominant in the presence of steam or oxygen at temperatures above 700 °C [3, 24]. Even at the initial step with Ar-sweep, an oxygen

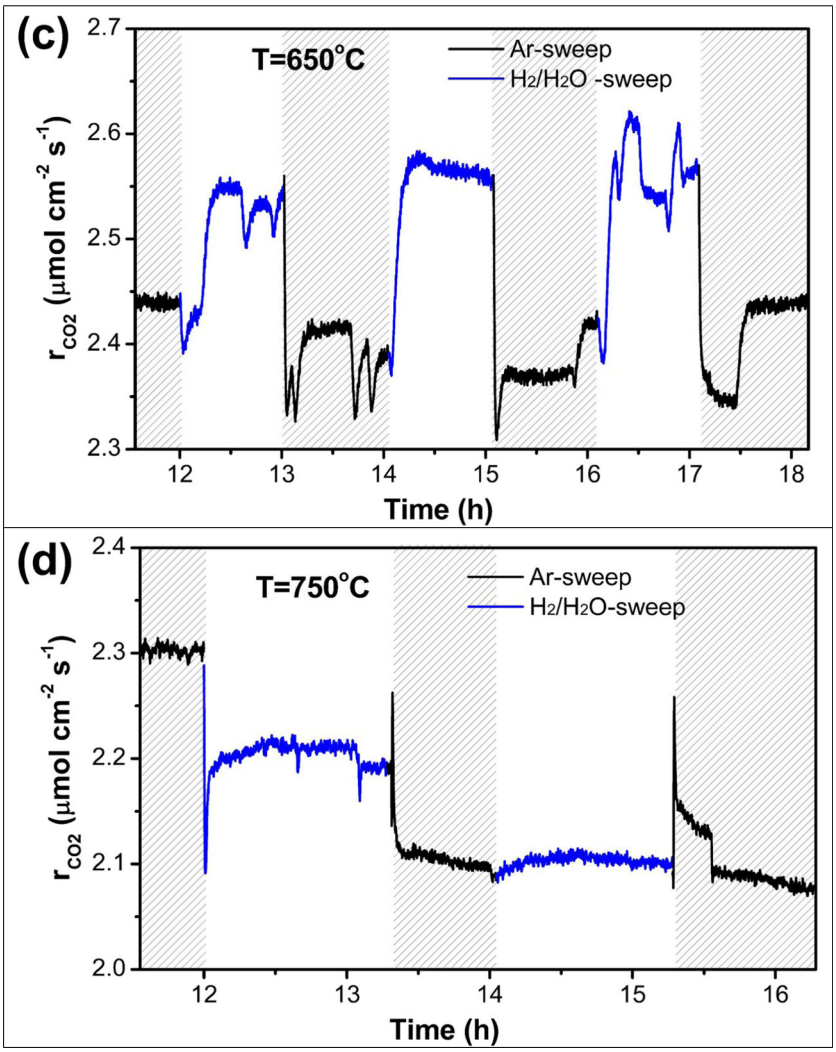

Fig. 10 continued.

chemical potential difference exists across the membrane due to the high oxygen excess in the reaction side. Hence, taking in account the increased oxygen ion conductivity of the membrane at this temperature, it is possible for adsorbed oxygen to be removed from the catalyst and transport through the membrane to the sweep side. Removal of oxygen ions from the catalytic surface would disfavour the adsorption of the electron donor (CO) which determines the reaction kinetics under these conditions. This is potentially a reason that the reaction rate during the initial step with Ar flow in the sweep side (2.3 μmol s^{-1} cm^{-2}) is lower than this of the corresponding stage at 650 °C (2.44 μmol s^{-1} cm^{-2}). During the next step of the cycle, the introduction of the H_2/H_2O-sweep creates hydrogen chemical potential gradient across the membrane which can activate proton transport from the sweep side to the reacting side, for an overall ambipolar diffusion of protons and oxygen ions. This means we now have two competing mechanisms that each could affect the reaction rate, but if oxygen flux is overall higher, the further decrease of the reaction rate can be explained. In the second and third cycles, it appears that these two competing mechanisms of conduction are in equilibrium and hence no further changes to the reaction rate are observed. However, it is difficult to provide any further interpretations for the catalytic rate changes under this very complex conducting behaviour.

Stability of the Pt/BCZ20Y20 membrane

The good chemical stability that BCZ20Y20 showed during the characterisation experiments of the powders was the main reason to be selected for the catalytic application. The reaction between BCZY and CO_2 takes place only at the gas-solid electrolyte interface and therefore a dense membrane would be expected to offer enhanced resistance to carbonation [35]. In addition, the stability of BCZY powder was proven under the exposure in a 100% CO_2 atmosphere, while during the catalytic experiments, the produced CO_2 inside the reactor was maintained at concentrations between 0.25 and 0.65%

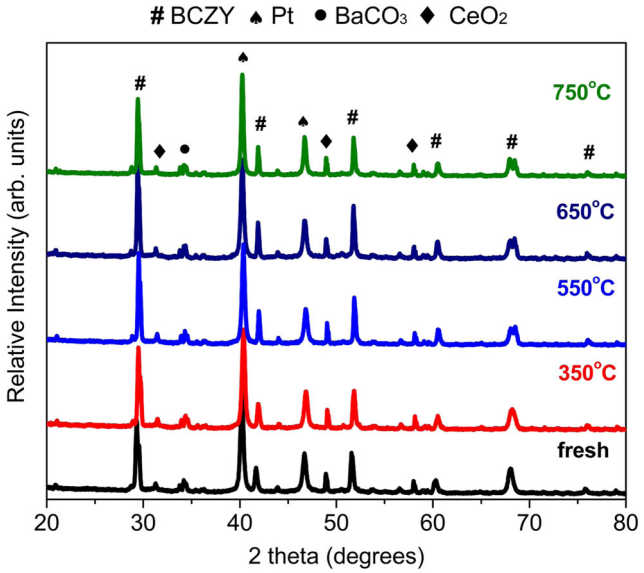

Fig. 11 XRD patterns of the Pt/BCZ20Y20 surface as prepared (black line) and after 24-h exposure at 350 °C (red line), 550 °C (light blue line), 650 °C and (blue line) and 750 °C (green line). Reactor conditions: pCO = 1 kPa, pO_2 = 10 kPa, f = 200 ml min^{-1}

of the total gas mixture. Figure 11 shows the XRD patterns for a Pt/BCZY surface of a duplicated membrane exposed in the same conditions, as the one used in the catalytic tests. Although the fresh membrane had minor impurities of CeO_2-like and $BaCO_3$ phases (probably due to the sintering and catalyst deposition procedures), the main perovskite phase was retained under these conditions and the relative intensity ratio between the BCZY peaks and the secondary phases peaks did not change. Hence, there was no sign of further decomposition observed for the BCZ20Y20. In addition, there was no indication of mechanical degradation for the tested membrane.

Conclusions

$BaCe_{1-x}Y_xO_{3-\delta}$ (BCY) and $BaCe_{0.8-y}Zr_yY_{0.2}O_{3-\delta}$ (BCZY) compounds were prepared by an aqueous sol-gel technique and calcined at 1100 °C and 1250 or 1400 °C, respectively. These materials were tested for their water uptake capability and stability in CO_2 as potential candidates for intermediate-temperature applications such as Electrochemical Promotion of Catalysis. Among the BCY compounds, the highest water uptake (related to the material's protonic conductivity) was obtained for this containing the highest Y-level, $BaCe_{0.8}Y_{0.2}O_{2.9}$ (BCY20), while the protonic defect concentration was higher than 80% for all the BCY samples during isothermal TGA measurements. Keeping Y-content in the B-site at 20%, further substitution of Ce^{4+} with Zr^{4+} was investigated in order to enhance the material's chemical stability without much expense in proton conductivity. Isothermal hydration TGA showed that Zr-doping gradually decreased the water uptake at 450 °C. Experiments for stability under CO_2 showed that $BaCe_{0.8-y}Zr_yY_{0.2}O_{3-\delta}$ (BCZY) compounds for $y \geq 0.2$ are stable for temperatures up to 450 °C and retain their perovskite structure even after heating up to 1000 °C, despite the harsh conditions were used in the work (p_{CO2} = 1 atm). Kinetic analysis for BCZY decomposition in CO_2 was performed by utilising two different methods and good agreement between the results was observed. Zirconium doping induced a decrease in the activation energy of the decomposition reaction; however, the reactivity was overall restricted as the pre-exponential factor was also decreased by several orders of magnitude for increasing Zr content.

Taking in account the hydration and stability properties of the tested materials, $BaCe_{0.6}Zr_{0.2}Y_{0.2}O_{3-\delta}$ was used for the wireless EPOC of CO oxidation on Pt. A modest rate modification was observed upon the introduction of protonic promoting species supply to the catalyst surface for temperatures up to 650 °C (where the material behaves predominantly as a proton conductor). The promotional effect on the catalytic rate was reversible and repeatable, showing that this membrane can effectively regulate the activity of the supported catalyst.

This preliminary work under reactive conditions using a wireless configuration (i.e. utilising the material's electronic mobility even at such low temperatures), in conjunction with the post-op XRD of BCZY powders, indicates that BCZY shows a lot of promise as a material in catalytic membrane reactors and applications involving reactions of environmental importance where H_2 transport required.

Acknowledgements The authors acknowledge financial support by the EPSRC (EP/M026159/1) and the Newton Fund Institutional Links scheme. Dr. Stavrakakis also acknowledges DEL NI for a PhD studentship.

References

1. Iwahara H, Esaka T, Uchida H, Maeda N (1981) Proton conduction in sintered oxides and its application to steam electrolysis for hydrogen production. Solid State Ionics 3–4:359–363. https://doi.org/10.1016/0167-2738(81)90113-2
2. Iwahara H (1996) Proton conducting ceramics and their applications. Solid State Ionics 86–88:9–15. https://doi.org/10.1016/0167-2738(96)00087-2

3. Bonanos N, Knight KS, Ellis B (1995) Perovskite solid electrolytes: structure, transport properties and fuel cell applications. Solid State Ionics 79:161–170. https://doi.org/10.1016/0167-2738(95)00056-C
4. Haile SM, Staneff G, Ryu KH (2001) Non-stoichiometry, grain boundary transport and chemical stability of proton conducting perovskites. J Mater Sci 36:1149–1160. https://doi.org/10.1023/A:1004877708871
5. Wienströer S, Wiemhöfer H-D (1997) Investigation of the influence of zirconium substitution on the properties of neodymium-doped barium cerates. Solid State Ionics 101–103:1113–1117. https://doi.org/10.1016/S0167-2738(97)00163-X
6. Ryu KH, Haile SM (1999) Chemical stability and proton conductivity of doped BaCeO3–BaZrO3 solid solutions. Solid State Ionics 125:355–367. https://doi.org/10.1016/S0167-2738(99)00196-4
7. Katahira K, Kohchi Y, Shimura T, Iwahara H (2000) Protonic conduction in Zr-substituted BaCeO3. Solid State Ionics 138:91–98. https://doi.org/10.1016/S0167-2738(00)00777-3
8. Schober T, Krug F, Schilling W (1997) Criteria for the application of high temperature proton conductors in SOFCs. Solid State Ionics 97:369–373. https://doi.org/10.1016/S0167-2738(97)00028-3
9. Zuo C, Zha S, Liu M, Hatano M, Uchiyama M (2006) Ba(Zr0.1Ce0.7Y0.2)O3–δ as an electrolyte for low-temperature solid-oxide fuel cells. Adv Mater 18:3318–3320. https://doi.org/10.1002/adma.200601366
10. Barison S, Battagliarin M, Cavallin T, Doubova L, Fabrizio M, Mortalò C, Boldrini S, Malavasi L, Gerbasi R (2008) High conductivity and chemical stability of BaCe1−x−yZrxYyO3−δ proton conductors prepared by a sol–gel method. J Mater Chem 18:5120. https://doi.org/10.1039/b808344d
11. Sawant P, Varma S, Wani BN, Bharadwaj SR (2012) Synthesis, stability and conductivity of BaCe0.8−xZrxY0.2O3−δ as electrolyte for proton conducting SOFC. Int J Hydrog Energy 37:3848–3856. https://doi.org/10.1016/J.IJHYDENE.2011.04.106
12. Yang S, Wen Y, Zhang S, Gu S, Wen Z, Ye X (2017) Performance and stability of $BaCe_{0.8-x}Zr_{0.2}In_xO_{3-\delta}$-based materials and reversible solid oxide cells working at intermediate temperature. Int J Hydrog Energy 42(47):28549–28558. https://doi.org/10.1016/j.ijhydene.2017.09.159
13. Zhong Z (2007) Stability and conductivity study of the $BaCe_{0.9-x}Zr_xY_{0.1}O_{2.95}$ systems. Solid State Ionics 178(3–4):213–220. https://doi.org/10.1016/j.ssi.2006.12.007
14. Guo Y, Lin Y, Ran R, Shao Z (2009) Zirconium doping effect on the performance of proton-conducting $BaZr_yCe_{0.8-y}Y_{0.2}O_{3-\delta}$ ($0.0 \le y \le 0.8$) for fuel cell applications. J Power Sources 193(2):400–407. https://doi.org/10.1016/j.jpowsour.2009.03.044
15. Chen CH, Kruidhof H, Bouwmeester HJM, Burggraaf AJ (1996) Preparation of gas-tight strontium-doped lanthanum cobaltate by an aqueous sol-gel process. Mater Sci Eng B 39:129–132. https://doi.org/10.1016/0921-5107(96)01582-6
16. Vernoux P, Lizarraga L, Tsampas MN, Sapountzi FM, de Lucas-Consuegra A, Valverde JL, Souentie S, Vayenas CG, Tsiplakides D, Balomenou S, Baranova EA (2013) Ionically conducting ceramics as active catalyst supports. Chem Rev 113:8192–8260. https://doi.org/10.1021/cr4000336
17. Tsiplakides D, Balomenou S (2008) Electrochemical promoted catalysis: towards practical utilization. Chem Ind Chem Eng Q 14:97–105. https://doi.org/10.2298/CICEQ0802097T
18. Poulidi D, Thursfield A, Metcalfe ISS (2007) Electrochemical promotion of catalysis controlled by chemical potential difference across a mixed ionic-electronic conducting ceramic membrane—an example of wireless NEMCA. Top Catal 44:435–449. https://doi.org/10.1007/s11244-006-0136-0
19. Poulidi D, Metcalfe ISS (2008) Comparative studies between classic and wireless electrochemical promotion of a Pt catalyst for ethylene oxidation. J Appl Electrochem 38(8):1121–1126. https://doi.org/10.1007/s10800-008-9525-3
20. Poulidi D, Metcalfe ISS (2010) In situ catalyst activity control in a novel membrane reactor—reaction driven wireless electrochemical promotion of catalysis. Chem Eng Sci 65(1):446–450. https://doi.org/10.1016/j.ces.2009.06.013
21. Poulidi D, Rivas ME, Zydorczak B, Wu Z, Li K, Metcalfe IS (2012) Electrochemical promotion of a Pt catalyst supported on La0.6Sr0.4Co0.2Fe0.8O3−δ hollow fibre membranes. Solid State Ionics 225:382–385. https://doi.org/10.1016/j.ssi.2012.03.010
22. Poulidi D, Anderson C, Metcalfe ISS (2008) Remote control of the activity of a Pt catalyst supported on a mixed ionic electronic conducting membrane. Solid State Ionics 179:1347–1350. https://doi.org/10.1016/j.ssi.2008.01.056
23. Poulidi D, Mather GCC, Metcalfe ISS (2007) Wireless electrochemical modification of catalytic activity on a mixed protonic-electronic conductor. Solid State Ionics 178:675–680. https://doi.org/10.1016/j.ssi.2007.02.022
24. Marrony M (2015) Proton-conducting ceramics: from fundamentals to applied research. Pan Stanford
25. Vayenas CG (2001) Electrochemical activation of catalysis: promotion, electrochemical promotion, and metal-support interactions. Springer Science & Business Media, Berlin
26. Della Negra M, Zhang W, Bonanos N, Ricote S (2014) Behavior of $BaCe_{0.9-x}Zr_xY_{0.1}O_{3-\delta}$ in water and ethanol suspensions. J Mater Sci 49:2588–2595. https://doi.org/10.1007/s10853-013-7955-8
27. Fabbri E, D'Epifanio A, Di Bartolomeo E et al (2008) Tailoring the chemical stability of $Ba(Ce_{0.8-x}Zr_x)Y_{0.2}O_{3-\delta}$ protonic conductors for Intermediate Temperature Solid Oxide Fuel Cells (IT-SOFCs). Solid State Ionics 179:558–564. https://doi.org/10.1016/J.SSI.2008.04.002
28. Shannon RD, IUCr (1976) Revised effective ionic radii and systematic studies of interatomic distances in halides and chalcogenides. Acta Crystallogr Sect A 32:751–767. https://doi.org/10.1107/S0567739476001551
29. Knight KS, Soar M, Bonanos N (1992) Crystal structures of gadolinium- and yttrium-doped barium cerate. J Mater Chem 2:709. https://doi.org/10.1039/jm9920200709
30. Li K (2007) Ceramic membranes for separation and reaction. John Wiley & Sons, Chichester
31. Kruth A, Irvine JTS (2003) Water incorporation studies on doped barium cerate perovskites. Solid State Ionics 162–163:83–91. https://doi.org/10.1016/S0167-2738(03)00252-2
32. Ricote S, Bonanos N, Caboche G (2009) Water vapour solubility and conductivity study of the proton conductor $BaCe_{(0.9-x)}Zr_xY_{0.1}O_{(3-\delta)}$. Solid State Ionics 180:990–997. https://doi.org/10.1016/J.SSI.2009.03.016
33. Oishi M, Akoshima S, Yashiro K, Sato K, Mizusaki J, Kawada T (2009) Defect structure analysis of B-site doped perovskite-type proton conducting oxide BaCeO3. Part 1: the defect concentration of BaCe0.9M0.1O3−δ (M = Y and Yb). Solid State Ionics 180:127–131. https://doi.org/10.1016/J.SSI.2008.12.025
34. Kreuer K (1999) Aspects of the formation and mobility of protonic charge carriers and the stability of perovskite-type oxides. Solid State Ionics 125:285–302. https://doi.org/10.1016/S0167-2738(99)00188-5
35. Norby T, Widerøe M, Glöckner R, Larring Y (2004) Hydrogen in oxides. Dalt Trans 0:3012–3018. https://doi.org/10.1039/B403011G
36. Meng W, Virkar AV (1999) Synthesis and thermodynamic stability of Ba2B′B″O6 and Ba3B*B″2O9 perovskites using the molten salt method. J Solid State Chem 148:492–498. https://doi.org/10.1006/JSSC.1999.8485
37. Bhide SV, Virkar AV (1999) Stability of $AB'_{1/2}B''_{1/2}O_3$-type mixed perovskite proton conductors. J Electrochem Soc 146:4386. https://doi.org/10.1149/1.1392648

38. Kissinger HE (1957) Reaction kinetics in differential thermal analysis. Anal Chem 29:1702–1706. https://doi.org/10.1021/ac60131a045
39. Budrugeac P, Segal E (2007) Applicability of the Kissinger equation in thermal analysis. J Therm Anal Calorim 88:703–707. https://doi.org/10.1007/s10973-006-8087-z
40. Jander W (1927) Reaktionen im festen Zustande bei höheren Temperaturen. Reaktionsgeschwindigkeiten endotherm verlaufender Umsetzungen, Zeitschrift für anorganische undallgemeine Chemie 163:1–30. https://doi.org/10.1002/zaac.19271630102
41. Okiba T, Fujishiro F, Hashimoto T (2013) Evaluation of kinetic stability against CO_2 and conducting property of $BaCe_{0.9-x}Zr_xY_{0.1}O_{3-\delta}$. J Therm Anal Calorim 113:1269–1274. https://doi.org/10.1007/s10973-013-3205-1
42. Kiskinova MP (1992) Poisoning and promotion in catalysis based on surface science concepts and experiments. In B. Delmon & J. T. Yates (Eds.), Studies in surface science and catalysis. 70:5. https://doi.org/10.1016/S1369-7021(04)00348-7
43. Thursfield A, Brosda, Pliangos C, Schober T, Vayenas CG (2003) Electrochemical promotion of an oxidation reaction using a proton conductor. Electrochimica Acta 48:3779–3788. https://doi.org/10.1016/S0013-4686(03)00511-57